Journal of Catalysis **191,** 301–317 (2000)
doi:10.1006/jcat.1999.2724, available online at http://www.idealibrary.com on IDEAL®

Electronic Factors Governing Ethylene Hydrogenation and Dehydrogenation Activity of Pseudomorphic Pd_{ML}/Re(0001), Pd_{ML}/Ru(0001), Pd(111), and Pd_{ML}/Au(111) Surfaces

Venkataraman Pallassana and Matthew Neurock[1]

Department of Chemical Engineering, School of Engineering and Applied Science, Thornton Hall, University of Virginia, Charlottesville, Virginia 22903

Received July 13, 1999; accepted October 14, 1999

DFT-GGA periodic slab calculations were used to examine the chemisorption, hydrogenation, and dehydrogenation of ethylene on pseudomorphic monolayers of Pd(111) on Re(0001) [Pd_{ML}/Re(0001)], Pd_{ML}/Ru(0001), Pd(111), and Pd_{ML}/Au(111). The computed ($\sqrt{3} \times \sqrt{3}$) di-σ binding energy for ethylene on Pd_{ML}/Re(00001), Pd_{ML}/Ru(0001), Pd(111), and Pd_{ML}/Au(111) are −10, −31, −62, and −78 kJ/mol, respectively. Hydrogen chemisorption follows trends very similar to the adsorption of ethylene with calculated dissociative adsorption energies of +2, −6, −78, and −83 kJ/mol, on the Pd_{ML}/Re(00001), Pd_{ML}/Ru(0001), Pd(111), and Pd_{ML}/Au(111) surfaces, respectively. The elementary reactions of ethylene hydrogenation to form a surface ethyl intermediate and the dehydrogenation of ethylene to form a surface vinyl species were examined as model reactions for metal-catalyzed coupling and adsorbate bond-breaking reactions, respectively. Activation barriers and energies of reaction were computed for these elementary C–H bond-forming and C–H bond-breaking reactions over all the aforementioned surfaces. Calculations indicate that the activation barriers for the C–H bond breaking of surface-bound ethylene and ethyl intermediates correlate linearly with the corresponding overall energies of reaction for different Pd overlayer surfaces, with a slope of 0.65. The C–H bond activation barriers appear to be lower on surfaces where the reaction is more exothermic, consistent with the Evans–Polanyi postulate. Finally, we demonstrate that both the trends in the adsorption energy of ethylene and the activation barriers for hydrogenation/dehydrogenation of ethylene are correlated to the intrinsic electronic properties of the bare metal surface. Using concepts derived from frontier-orbital theory, we extend the simple surface-activity model developed by Hammer and Nørskov (*Surf. Sci.* 343, 211 (1995)) to predict the chemisorption and surface reactivity of both ethylene and ethyl on different surfaces. The d-band for the bare Pd overlayer is observed shifting closer to the Fermi energy as the substrate metal is changed from a reactive metal such as Re to a noble metal such as Au. Since C–H bond activation of ethyl and ethylene is primarily guided by electron-backdonation to the antibonding σ_{CH^*} orbital, the activation barriers for C–H bond breaking were found to be lower on surfaces where the d-band is closer to the Fermi level. The converse is true for the microscopic reverse, C–H bond formation reaction. © 2000 Academic Press

Key Words: **ethylene; hydrogenation; dehydrogenation; bimetallic overlayers; palladium; chemisorption; ethyl; vinyl; density functional theory; Evans–Polanyi relation; LFER.**

1. INTRODUCTION

The transformation of chemical species on a transition metal surface is typically brought about by a series of elementary adsorbate bond-breaking and coupling steps. It is well-known that transition metals to the left of the periodic table form strong metal–adsorbate bonds due to vacancies in the valence d-band. Adsorbate dissociation increases the number of metal–adsorbate bonds and is therefore thermodynamically favored on these metals. For example, CO readily dissociates on metals such as Mo and W that are to the left of the periodic table, while it is molecularly adsorbed on metals such as Pd, Pt, and Au, which are situated at the right end of the transition metal series (1). While bond-breaking activity is often required in metal catalysts, complete decomposition of organic reactants can lead to coking of the catalyst surface. The completion of a catalytic cycle also requires desorption of the products. This desorption step is, in most cases, preceded by the recombination of product fragments on the catalyst surface. Reactive metals such as Mo and Re, which form strong metal–adsorbate bonds, are not as efficient for such coupling reactions. A delicate balance between bond-scission and fragment-coupling activity is therefore required to complete the sequence of elementary steps that comprise the overall catalytic cycle. This generalized concept of catalytic reactivity was recognized by Sabatier in the early half of the 20th century and is commonly referred to as the Sabatier principle (2).

[1] Author to whom correspondence should be addressed. Mailing address: Rm. 117 A, Department of Chemical Engineering, School of Engineering and Applied Science, Thornton Hall, Mc Cormick Road, Charlottesville, VA 22903. Fax: (804) 982 2658.

0021-9517/00 $35.00

An optimal trade-off between adsorbate bond-breaking and fragment-recombination functionality is often achieved by using a bimetallic catalyst composed of reactive and noble metals. Steam reforming of methane (Ni–Au), Fischer–Tropsch synthesis (Ni–Co), aromatics production (Pt–Re), and tetrahydrofuran synthesis (Pd–Re or Ru–Re) are just a few examples of commercially relevant processes that employ bimetallic catalysts (3–6). Understanding the role of bimetallic metal–metal interaction on chemical reactivity in such systems is likely to aid the development of new catalytic materials.

In recent years, surface scientists have successfully synthesized and characterized well-defined bimetallic overlayers and alloyed surfaces under ultrahigh vacuum (UHV) conditions (7–18). Advances in computational quantum-chemical techniques and computer hardware are also making it possible to model the surface reactivity of these idealized bimetallic surfaces (19–24). Through theory and experiment, it is now possible to probe the reactivity of a well-structured bimetallic surface at the atomic level. In this paper, we use density functional theory to examine the intrinsic electronic properties of bimetallic, pseudomorphic overlayer surfaces and their effects on C–H bond-breaking and C–H bond-making activity. To accomplish this, we consider the reactions of ethylene on pseudomorphic monolayers of Pd on close-packed surfaces of Re, Ru, Pd, and Au. The coupling reaction of interest here is the surface reaction of ethylene and atomic hydrogen to form a surface ethyl intermediate. Metal-induced adsorbate bond-breaking is examined by studying the dehydrogenation of ethylene to form a surface vinyl species.

1.1. Ethylene Hydrogenation versus Decomposition on Metal Surfaces

The adsorption, hydrogenation, and thermal decomposition of ethylene has been experimentally studied on a number of well-defined single-crystal surfaces including Pd(100) (25, 26), Pd(111) (27, 28), Pd(110) (29, 30), Fe(100) (31), Pt(111) (32–34), Ag(111) (35), and Rh(111) (36). Depending upon the reaction conditions and the nature of the surface, it is known that ethylene can either selectively hydrogenate to ethane or decompose to form species such as ethylidyne and other C_xH_y intermediates (37). Under some conditions and over certain metals, both hydrogenation and dehydrogenation reactions occur with comparable rates. While there is a wealth of experimental data on the reactivity of chemisorbed ethylene on various different metal surfaces, a fundamental understanding of how the intrinsic properties of the surface control olefin hydrogenation versus dehydrogenation activity is still premature. In this paper, we begin to address this issue by analyzing the changes in the activation barrier for hydrogenation and dehydrogenation of ethylene due to changes in the electronic properties of the metal surface.

The detailed reaction pathways for ethylene decomposition on a metal surface are quite complex (34–36, 38, 39), and a comprehensive analysis of all pathways is beyond the scope of this work. We consider here the initial elementary activation steps in the hydrogenation and dehydrogenation of ethylene. The first involves the hydrogenation of ethylene to form surface-bound ethyl. The second elementary reaction is the dehydrogenation of ethylene to form vinyl. These are used herein, as model reactions to characterize the hydrogenation versus dehydrogenation activity of the metal surface.

1.2. Hydrogenation of Ethylene to Surface Ethyl on Pd(111)

The hydrogenation of ethylene has been studied extensively on different single-crystal surfaces as a model for olefin hydrogenation (29, 32, 40, 41). Detailed experiments have confirmed that the reaction proceeds via the Horiuti–Polanyi mechanism with the formation of an ethyl surface intermediate (42–44). More recent sum frequency generation (SFG) experiments on Pt(111) indicate that while the surface is primarily covered with di-σ-bound ethylene, the π-bound ethylene species may be more important for hydrogenation activity (32). On palladium, however, it is not known whether hydrogenation of the π or di-σ species dominates the surface. In an early study for ethylene hydrogenation over Pd(111) we found that repulsive interactions between π-bound ethylene and atomic hydrogen force ethylene into the di-σ-bound mode, at low surface coverages (45–47). Hydrogenation of the di-σ-bound ethylene appeared to be the only stable reaction pathway at low surface coverage. More recently, however, we found that, at higher surface coverages, hydrogenation of the π-bound ethylene has a lower activation barrier and may be more preferable (45–47). In this work, we uncouple the intrinsic reactivity from coverage effects and examine the hydrogenation of the di-σ ethylene, which is the more favorable intermediate at low coverage.

The DFT-calculated reaction pathway for the hydrogenation of ethylene to ethyl on Pd(111) is shown in Fig. 1 (45, 46). The hydrogenation of ethylene to ethyl involves the insertion of a surface atomic hydrogen into the Pd–C bond to form a new C–H bond. The mechanism is more easily analyzed by examining the reverse step, which from microscopic reversibility is the β-hydride elimination reaction. The electronic interactions involved in the C–H bond activation of the ethyl intermediate on Pd(111) are illustrated in Fig. 2. Figure 2 (see lowermost frame) shows the density of states projected to the β-carbon 2*p* and hydrogen 1*s* states of ethyl in vacuum. The states located below and above the Fermi energy at -6.0 and $+5.0$ eV correspond to the σ_{CH} (bonding) and σ^*_{CH} (antibonding) orbitals, respectively. For ethyl on Pd(111), these orbitals do not interact with the metal. The β-hydride elimination step involves an

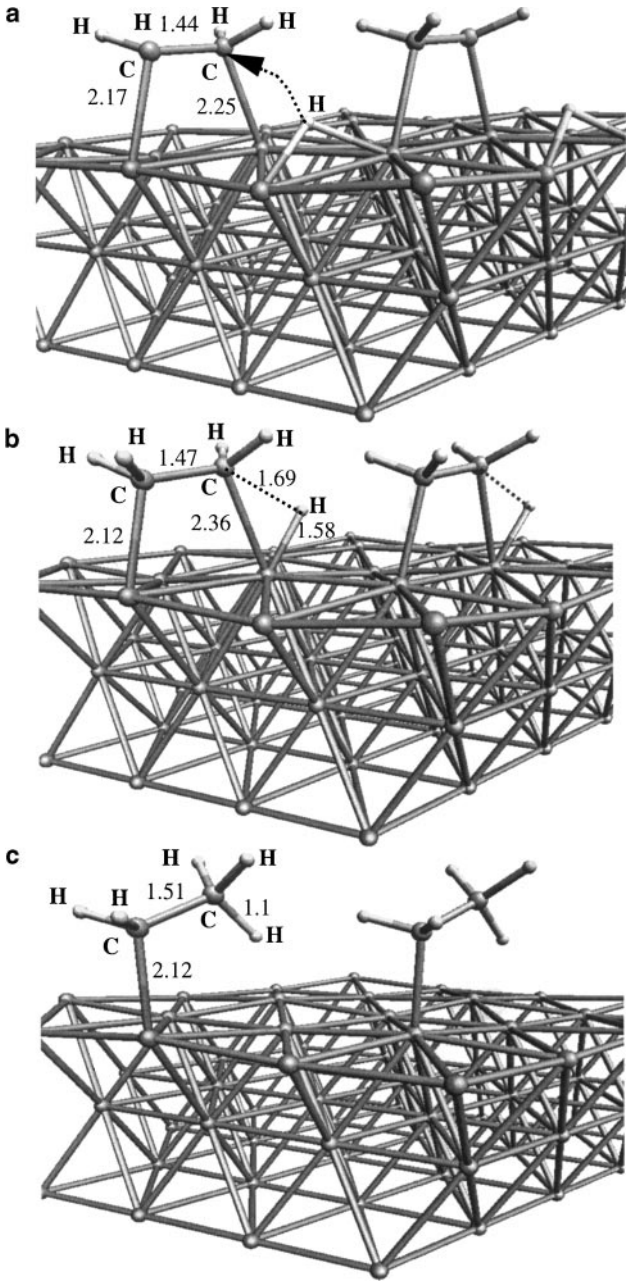

FIG. 1. DFT-computed reaction pathway for ethylene hydrogenation to a surface ethyl species on Pd(111). (a) Di-σ-bound ethylene and hydrogen on Pd(111); (b) transition state; (c) ethyl on Pd(111).

agostic stretch of the C–H bond. As the C–H bond is elongated, the overlap between the carbon (sp^3 hybrid orbital) and H (1*s* orbital) is reduced. Consequently, the energy gap between the σ_{CH} and σ_{CH^*} states is reduced, and these orbitals shift closer to the Fermi energy. At the transition state, the σ_{CH} and σ_{CH^*} orbitals begin to interact with the valence s-, p-, and d-states of the metal, resulting in electron donation and backdonation interaction states (as is seen in the second panel of Fig. 2). This interaction is stronger for the σ^*_{CH} state with the metal d-band, as compared to that for the σ_{CH} state. In other words, the C–H bond activation of ethyl is primarily guided by the backdonation of electrons from the metal into the antibonding σ_{CH^*} state of ethyl (48). The DFT-computed C–H bond distance at the transition state geometry for this reaction is 1.7 Å (refer to Fig. 1). The transition state is late along the reaction coordinate for ethyl C–H bond activation. From Fig. 1, there appears to be a significant level of Pd–H and Pd–C bond formation at the transition state. These results are consistent with previously reported theoretical results for the C–H bond activation of species such as acetate on Pd(111) and methane and ethyl on Ni (49–53).

1.3. Dehydrogenation of Ethylene to Vinyl on Pd(111)

The dehydrogenation of ethylene to vinyl is speculated to be a single elementary step (25), although the vinyl species has never actually been identified on the Pd(111) and Pt(111) surfaces (27, 38). This may be because species such

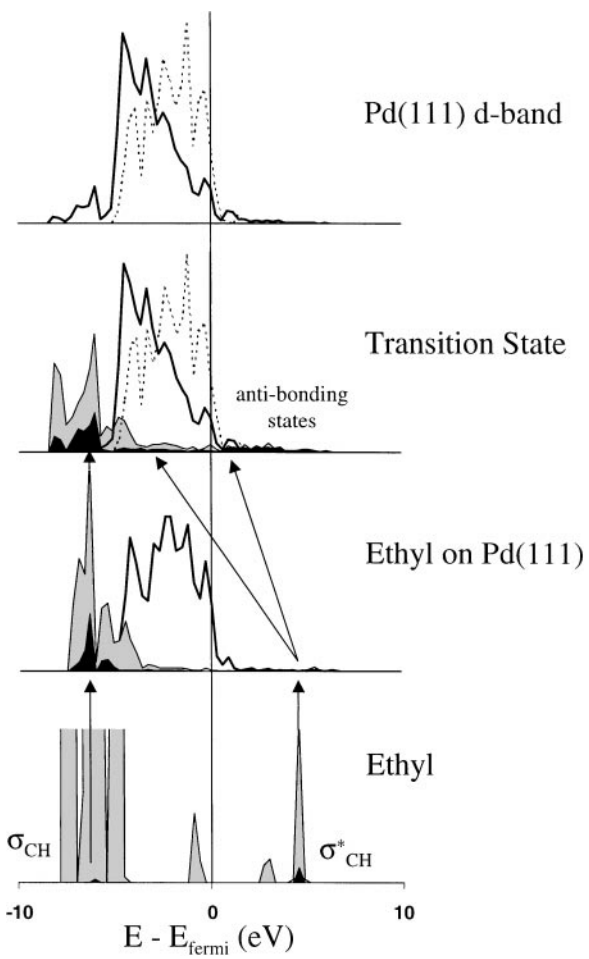

FIG. 2. Frontier orbital interactions for C–H bond activation of ethyl on Pd(111). Shaded areas indicate density of states (DOS) projected to carbon 2*p* and hydrogen 1*s* states of the β C–H bond. Solid line corresponds to DOS projected to Pd d-band for the adsorbate–metal system. The bare surface Pd d-band (dotted line) is shown for comparison.

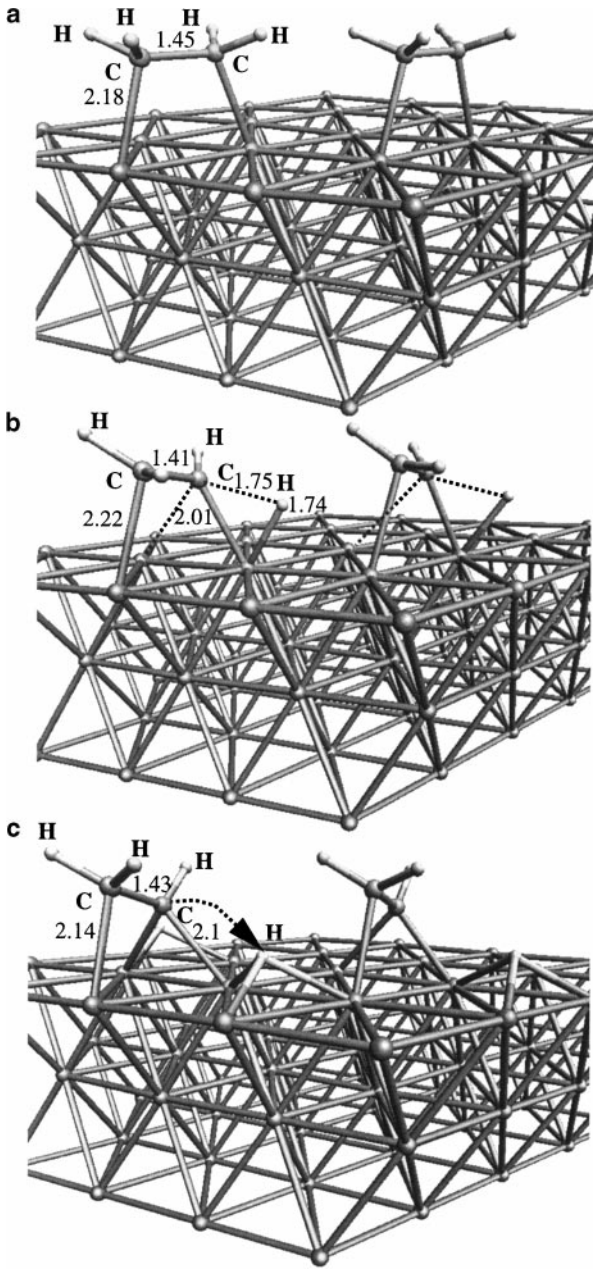

FIG. 3. DFT-computed reaction pathway for ethylene dehydrogenation to a surface vinyl species on Pd(111). (a) Di-σ-bound ethylene on Pd(111); (b) transition state; (c) $\eta^1\eta^2$-bound vinyl and 3-fold hydrogen on Pd(111).

as ethylidyne and ethylidene are much more stable than vinyl on the (111) hexagonal facets. Vinyl has been observed to be stable, however, on the Pd(100) surfaces (25). It has been speculated that di-σ-bound ethylene is the reactive intermediate for vinyl formation (25, 40).

Figure 3 shows the reaction pathway for the dehydrogenation of ethylene to vinyl on a Pd(111) surface, as determined using DFT calculations. The reaction coordinate for C–H bond breaking of ethylene bears close semblance to that of ethyl β-hydride elimination. Similar to ethyl C-H bond activation, the dehydrogenation of ethylene involves the interaction of the σ_{CH} and σ_{CH^*} orbitals of ethylene with the metal. Following an agostic stretch of the C–H bond, electron backdonation into the anti-bonding σ^* orbital causes weakening of the C–H bond, ultimately breaking it. C–H bond scission in this case also occurs over a single surface metal atom. Remarkably, the C–H bond distance (1.75 Å) at the transition state is nearly the same as that found for ethyl C–H bond activation. The transition state for this reaction is situated late along the reaction coordinate for ethylene dehydrogenation. The primary difference between ethylene and ethyl C–H bond activation involves the concerted torsion of the C=C–Pd–Pd dihedral angle, from 0° to 30°, during the C–H bond breaking of ethylene. This torsion is necessary because the resulting vinyl species is most favorably bound in the $\eta^1\eta^2$ mode (see lowermost panel in Fig. 3).

2. COMPUTATIONAL DETAILS

Nonlocal gradient-corrected, density functional calculations were used to determine all the structural and energetic results discussed in this paper. All calculations were performed using a full, periodic slab geometry to represent the metal surface. In cluster calculations, the molecular orbitals are generally localized to a finite region in three-dimensional space. They are therefore approximated by a linear combination of atom-centered Gaussian- or Slater-type functions, which constitute the atomic orbital basis set. In the periodic slab, the metal eigenstates close to the Fermi level are best described by Bloch functions (54, 55). The valence eigenstates are therefore approximated by a linear combination of a plane wave basis set with a maximum kinetic energy of 40 Ry (56). For our calculations, it was ensured in a few cases that the total energy of the system did not change by increasing the cutoff energy beyond 40 Ry. The core orbitals are described by frozen-core, scalar-relativistic, norm-conserving pseudopotentials (57). The exchange-correlation potential used in the local density approximation is of the functional form proposed by Vosko, Wilk, and Nusair (58). Nonlocal contributions to the exchange-correlation energy were incorporated self-consistently while the Kohn–Sham equations were solved (59, 60), using the Perdew–Wang (PW91) functional (61).

For ethylene on Pd(111), a $(\sqrt{3} \times \sqrt{3})$ unit cell was found to provide an optimal balance to minimize the size of the unit cell without encountering strong adsorbate–adsorbate repulsive interactions (50). Eighteen Chadi–Cohen special k-points were found to be adequate for sampling the first Brillouin zone corresponding to this $(\sqrt{3} \times \sqrt{3})$ super cell in real space (62). Hydrogen adsorption was examined for a (1×1) unit cell. Fifty-four Chadi–Cohen special k-points were found to be adequate for the first Brillouin zone sampling in this case (62).

The description of wavefunctions, in the direction perpendicular to the slab by a finite number of plane waves, requires the periodic repetition of the slabs normal to the surface. The slab periodicity perpendicular to the surface was chosen appropriately to eliminate interactions between adjacent slabs. A vacuum region of thickness corresponding to five metal layers was found to be adequate for this purpose. Electronic occupations were Fermi-distributed with an electronic $k_BT = 0.1$ eV to stabilize the electronic convergence scheme, but all final total energies were extrapolated back to 0 K (63). Since the metal surfaces examined here are nonmagnetic in the bulk, all slab calculations were performed spin-unpolarized. Calculations were performed using the DACAPO program developed at the Technical University of Denmark (64, 65).

Transition states for C–H bond-breaking of ethyl and ethylene were determined using reaction coordinate calculations on a cluster model of the Pd(111) surface (45, 46). For the C–H bond-breaking reactions, the principal component to the reaction coordinate is along the C–H bond stretch. The C–H bond stretch was, therefore, chosen as a starting reaction coordinate to locate the transition state. The first step in our transition state search procedure was to map out a series of structures, having C–H bond distances intermediate to the reactant and product. At each of these structures, the geometry was partially optimized by minimizing the energy of the system along all internal modes except the C–H bond distance, which was kept constrained during the optimization procedure. This constrained geometry optimization scheme provided a series of structures and energies along the chosen trial reaction coordinate. The point of maximum energy along the trial coordinate provided a better guess for the transition state geometry. Detailed transition state search algorithms were employed to refine the transition state geometry, such that the energy gradients along all internal modes were close to zero. Vibrational frequencies were computed at the resulting transition state structure, to verify the existence of a negative eigenmode, corresponding to the reaction coordinate. Transition states for ethyl and ethylene C–H bond breaking were re-optimized for all the pseudomorphic, Pd(111) overlayer slabs, using the cluster-optimized transition state as an initial guess structure. The calculation of forces in the periodic slab geometry, using the cluster-optimized transition state as a trial structure, indicated that the forces on the atoms were very small in all directions, except in the direction perpendicular to the slab. The transition state geometry was therefore re-optimized to minimize the forces along this direction. At the final slab-optimized transition state structure, the forces in all directions were within the convergence threshold of 0.2 eV/Å. A comparison of the cluster-optimized geometries with the periodic slab structures showed very little differences for the adsorbate C–C and C–H bond distances. The metal–C and metal–H bond distances in the slab calculations, however, were observed to be consistently shorter (∼0.1 Å) than the corresponding distances in the cluster optimized geometry. This is most likely because of the different pseudopotentials and basis functions used in the cluster and slab calculations.

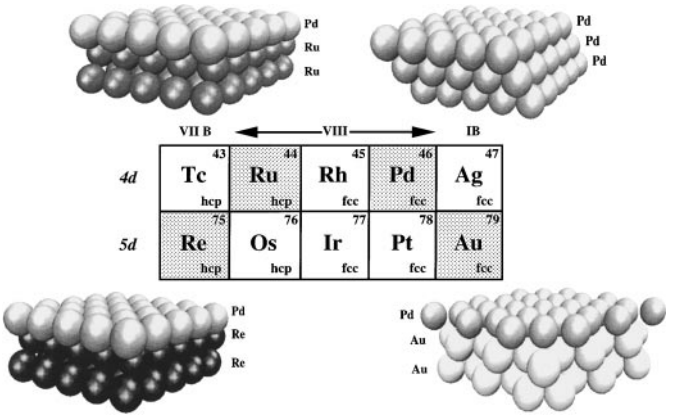

FIG. 4. Pseudomorphic Pd overlayers examined in this study. The lightly shaded elements on the periodic table indicate the substrate metals studied in this paper.

The surfaces examined in this study are depicted in Fig. 4. Each slab is composed of three metal layers, the lower two belonging to the substrate metal (Re, Ru, Pd, or Au) and the top layer being Pd in all cases. Previously, we showed that a three-layer slab model is adequate to predict reasonable adsorption energetics for adsorbates such as ethylene and hydrogen (23, 50). The substrate metals were chosen so as to span a set of elements across the periodic table, which have a different number of valence d-electrons. The choice of surfaces was also motivated by the fact that these surfaces have been studied experimentally under UHV conditions (7, 9, 10, 27, 66, 67). The surfaces examined are the close-packed surfaces for the substrate metal. For hcp metals Re and Ru, the (0001) plane has the highest surface atom density. Similarly, for fcc elements Pd and Au, the (111) facet is most closely packed. The Pd overlayer was initially placed at the idealized pseudomorphic position corresponding to the substrate and was subsequently optimized. It has been reported that the growth of the Pd overlayer, on all of the substrates analyzed here, occurs in a layer-by-layer fashion described by the Frank–van der Merwe mode (7, 10, 67). Surfaces with a pseudomorphic monolayer of Pd on substrates such as Re and Ru are observed to be thermally stable at high temperatures, with minimal alloying of the surface and substrate layers (7). $Pd_{ML}/Au(111)$, on the other hand, is stable only at very low temperatures (9, 10). At 300 K, significant intermixing of the Pd overlayer and the Au substrate is observed (9, 10). In this study, we only examine the pseudomorphic overlayers. The metal–metal distance within each layer was set to the experimental interatomic distance for the substrate metal. For Re, Ru, Pd, and Au, the interatomic distances are 2.76, 2.71, 2.75, and 2.88 Å,

respectively (54). All structural variables for the adsorbate and the slab were optimized, with the exception of the lowermost layer of the slab, which was intentionally fixed to the bulk lattice parameter.

3. RESULTS

3.1. Ethylene and Hydrogen Chemisorption

The ($\sqrt{3} \times \sqrt{3}$) periodic adsorption of ethylene was examined on the Pd_{ML}/Re(0001), Pd_{ML}/Ru(0001), Pd(111), and Pd_{ML}/Au(111) surfaces using DFT-GGA slab calculations. Table 1 summarizes the DFT-optimized geometric parameters and binding energies for ethylene on all the surfaces. The adsorption of ethylene is least favorable on Pd_{ML}/Re(0001) with a very weak binding energy of −10 kJ/mol. The computed adsorption energy for ethylene on Pd_{ML}/Ru(0001) is −31 kJ/mol, which is slightly higher than that on Pd_{ML}/Re(0001). Although we have not been able to find experimental estimates for ethylene adsorption on these surfaces, Koel and co-workers have demonstrated experimentally that ethylene binds more weakly to Pd monolayers on the Mo(100) surface as compared to Pd(111) (68). It is also well established that molecular adsorbates, such as CO, bind more weakly on the bimetallic Pd_{ML}/Re(0001) and Pd_{ML}/Ru(0001) surfaces in comparison to monometallic Pd(111) (7, 8, 66). Campbell *et al.* report that the CO desorption temperatures from the Pd_{ML}/Re(0001) and Pd_{ML}/Ru(0001) surfaces are 110 and 125 K, respectively, lower than that from the monometallic Pd(111) surface (7). XPS measurements indicate that there is a shift in the energy of the Pd ($3d^{5/2}$) electron to a higher binding energy due to the presence of the Re or Ru bulk (7, 8, 66). Hammer and Nørskov theoretically demonstrate a corresponding shift in the valence d-band for these pseudomorphic Pd monolayers (21, 69). This shift to a higher electron binding energy indicates that there are strong Pd–Re and Pd–Ru interactions, resulting in the weakening of the adsorbate interaction energy with the Pd overlayer. A detailed analysis of the electronic factors determining the changes in adsorption energies is presented in Section 4.2.

In contrast to these surfaces, the adsorption of ethylene on Pd(111) is significantly stronger, with a binding strength of −62 kJ/mol. The DFT-calculated result is in good agreement with previously computed theoretical values (−60 and −55 kJ/mol) (70, 71) and experimental TPD estimates (−59 kJ/mol) (27, 72). Amongst all the surfaces examined in this paper, the adsorption of ethylene is strongest on the bimetallic Pd_{ML}/Au(111) surface, with a binding energy of −78 kJ/mol. Koel and co-workers have studied the adsorption of CO on Pd_{ML}/Au(111) and have determined that the binding energy of CO on the Pd_{ML}/Au(111) is comparable to that on Pd(111) (9). At 300 K, however, the Pd overlayer and the Au substrate begin to intermix, forming surface alloys and rendering the experimental analysis difficult (9, 10).

Table 1 tabulates the optimized structural parameters important in ethylene di-σ chemisorption on each of the metal surfaces. Although the direct interaction of ethylene is with the Pd overlayer in all cases, there are noticeable differences in the Pd–carbon (Pd–C) bond distances for the different surfaces. The Pd–C bond distances appear to correlate here with the metal adsorbate bond strengths. For instance, the Pd–C bond distance is shortest (2.14 Å) on Pd_{ML}/Au(111), where ethylene is most strongly bound. The same bond is about 0.15 Å longer on Pd_{ML}/Re(0001), which exhibits the weakest interaction with ethylene. The calculated C–C bond distance for vapor-phase ethylene and ethane are 1.34 and 1.54 Å, respectively. The C=C bond length for di-σ-bonded ethylene is observed to increase on surfaces that exhibit stronger adsorption energies (Table 1). This is commensurate with a decreasing C=C bond order due to rehybridization of the valence orbitals on carbon from sp^2 to sp^3 during di-σ adsorption. The longer C–C bond distance on Pd_{ML}/Au(111) may also be partly due

TABLE 1

Geometric Parameters and Energies for Ethylene and Hydrogen Chemisorption on Pd(111) and Pseudomorphic Monolayer of Pd(111) on Re(0001), Ru(0001), and Au(111)

Surface	ΔE_{ads} C_2H_4 (kJ/mol)[a]	Pd–C (Å)	C=C (Å)	Binding energy (H) (kJ/mol)	ΔE_{ads} H_2 (kJ/mol)[b]	Pd–H (Å)	Lateral interaction energy (kJ/mol)[c]
Pd_{ML}/Re(0001)	−10	2.30	1.39	−217	+2	1.85	+12
Pd_{ML}/Ru(0001)	−31	2.25	1.41	−221	−6	1.80	+18
Pd(111)	−62	2.19	1.45	−257	−78	1.80	+18
Pd_{ML}/Au(111)	−78	2.14	1.45	−260	−83	1.83	+15

[a] Binding energy of ethylene on bare metal surface for ($\sqrt{3} \times \sqrt{3}$) adsorption.
[b] Energy for dissociative adsorption of H_2. Coverage = 100% fcc sites.
[c] Based on ethylene and hydrogen ($\sqrt{3} \times \sqrt{3}$) coadsorption. Lateral interaction energy is per C_2H_4–H pair.

to the increased lattice Pd–Pd distance for this surface (2.88 Å).

The binding of atomic hydrogen was also examined on all the surfaces of interest in this paper. Atomic hydrogen prefers the 3-fold fcc site on Pd(111) (23, 73–75). The adsorption of hydrogen was studied at 100% coverage of the 3-fold fcc sites. The lateral interactions between adsorbed hydrogen atoms on Pd are rather weak. At 100% coverage of H on Pd(111) the repulsive interactions were found to be within 20 kJ/mol and were predominantly due to through-space interactions between the hydrogen atoms (23, 74). The through-space adsorbate–adsorbate interactions are less dependent on the nature of the surface and are, therefore, very easy to correct, to calculate the low-coverage adsorption energies. The calculated trends in the binding energy at 100% coverage, reported here, are also expected to be valid for a lower surface coverage of hydrogen.

The DFT-calculated binding energy of atomic hydrogen on Pd_{ML}/Re(0001), Pd_{ML}/Ru(0001), Pd(111), and Pd_{ML}/Au(111) are −217, −221, −257, and −260 kJ/mol, respectively. Accounting for the H–H bond dissociation energy in the vapor phase (+436 kJ/mol) (76), the energy of dissociative adsorption of H_2 on the Pd_{ML}/Re(0001), Pd_{ML}/Ru(0001), Pd(111), and Pd_{ML}/Au(111) surfaces are estimated to be +2, −6, −78, and −83 kJ/mol, respectively. The DFT-computed adsorption energy for hydrogen on Pd(111) is in good agreement with previously reported theoretical (73, 75, 77) and experimental (78) values. It is interesting to note that the dissociative adsorption of H_2 on Pd_{ML}/Re(0001) and Pd_{ML}/Ru(0001) is almost thermoneutral. Hammer and Nørskov have shown that the activation barriers for dissociative chemisorption of H_2 on surfaces appear to correlate with the overall chemisorption energies (69, 79, 80). For surfaces such as Cu(111), where H_2 dissociative chemisorption is weakly exothermic, the adsorption process is activated with a barrier of about 50 kJ/mol (79, 80). Based on this observation, it is likely that the adsorption of H_2 is also activated on the Pd_{ML}/Re(0001) and Pd_{ML}/Ru(0001) surfaces.

DFT calculations indicate that the dissociative adsorption of H_2 on the Pd(111) and Pd_{ML}/Au(111) surfaces are exothermic by −78 and −83 kJ/mol, respectively. Dissociative hydrogen chemisorption is known to be nonactivated on Pd(111) (79). Since atomic hydrogen is slightly more strongly bound to Pd_{ML}/Au(111), it is unlikely to have a barrier on this surface. Table 1 shows the optimized metal–hydrogen (M–H) bond distance for the binding of a single hydrogen atom to the 3-fold fcc site. The M–H bond distance is roughly 1.8 Å for all the surfaces studied here. It is slightly longer on the Pd_{ML}/Re(0001) surface, which is consistent with the weaker interaction of hydrogen on this surface. The slightly longer M–H distance on the Pd_{ML}/Au(111) surface is most likely due to the larger lattice parameter for this surface (2.88 Å) as compared to that of Pd(111) (2.75 Å). It is important to note that the trends in ethylene adsorption energies and atomic hydrogen chemisorption energies on all the surfaces examined in this paper are very similar. Both ethylene and hydrogen are very strongly bound on the Pd_{ML}/Au(111) surface and most weakly bound on the Pd_{ML}/Re(0001) surface.

The hydrogenation of ethylene to a surface ethyl intermediate requires the coadsorption of ethylene and hydrogen at adjacent sites, by the sharing of surface metal atoms. Lateral interactions between the two adsorbates are likely to influence the adsorption energies of both species. To estimate the lateral interaction energies between C_2H_4 and H, the coadsorption of these two species was examined for a $(\sqrt{3} \times \sqrt{3})$ coverage on all the surfaces. For a $(\sqrt{3} \times \sqrt{3})$ structure, each di-σ-bound ethylene species has two nearest neighbor hydrogen atoms. The lateral interaction energy per ethylene–hydrogen pair was therefore estimated as half the difference in the adsorption energy of ethylene on the surface, with and without preadsorbed hydrogen. The lateral interaction energies thus calculated are listed in Table 1. It appears that the interaction energies between ethylene and hydrogen are 12–18 kJ/mol repulsive and show relatively weak dependence on the nature of the substrate.

3.2. *Hydrogenation of Di-σ-Bound Ethylene to Ethyl*

In section 1.2 we described the reaction pathway for the hydrogenation of ethylene from the di-σ-adsorbed mode. In this section, the reaction energetics for the hydrogenation of ethylene to ethyl on the various pseudomorphic $Pd_{ML}/M(111)$ (M = Re, Ru, Pd, and Au) surfaces are discussed. Table 2 summarizes the activation barrier and energy of reaction for the hydrogenation of ethylene to ethyl on the Pd overlayer with different substrates. DFT calculations indicate that the hydrogenation of ethylene to ethyl is almost *thermoneutral* on the Pd(111) surface. The same reaction is *exothermic* by −48 kJ/mol on the Pd_{ML}/Re(0001) surface and exothermic by −34 kJ/mol on the Pd_{ML}/Ru(0001) surface. Interestingly, the hydrogenation reaction is *endothermic* on the Pd_{ML}/Au(111) surface with an energy of reaction of +32 kJ/mol.

In Fig. 5, we plotted the DFT-computed binding energy of atomic hydrogen, ethylene, and surface ethyl on the different surfaces examined here. It is interesting to observe that the binding energies of all three species show very similar trends. They are all strongly bound on the Pd_{ML}/Au(111) surface and weakly adsorbed on the Pd_{ML}/Re(0001) surface. The hydrogenation reaction involves the coupling of surface-bound ethylene and hydrogen to form a surface ethyl intermediate. It follows that the differences in the overall reaction energies for the hydrogenation of ethylene to surface ethyl are, therefore, likely to follow the changes in the adsorption energy of ethylene, on the various pseudomorphic overlayers.

TABLE 2

Activation Barriers and Energy of Reaction for Ethylene Hydrogenation to Ethyl on Pd(111) and Pseudomorphic Monolayers of Pd(111) on Re(0001), Ru(0001), and Au(111) ($C_2H_4^* + H^* \underset{k_r}{\overset{k_f}{\rightleftharpoons}} C_2H_5^* + *$)

Surface	ΔE_{rxn} (kJ/mol) hydrogenation	ΔE_{act}^{f} (kJ/mol) hydrogenation	ΔE_{act}^{r} (kJ/mol) β-hydride elimination	Geometric parameters at transition state		
				C–H (Å)	Pd–H (Å)	Pd–C (Å)
Pd_{ML}/Re(0001)	−48	+78	+126	1.74	1.59	2.44
Pd_{ML}/Ru(0001)	−34	+77	+111	1.72	1.59	2.44
Pd(111)	0	+82	+82	1.69	1.56	2.31
Pd_{ML}/Au(111)	+32	+104	+72	1.66	1.55	2.33

Activation barriers for hydrogenation were determined by optimizing the reactant, transition state, and products for ethylene hydrogenation individually on each of the surfaces and computing the difference in the total energy between the transition state and the reactant state. The activation barriers for the microscopic reverse reaction of β-hydride elimination of the surface ethyl intermediate are also listed in Table 2.

The geometric parameters along the reaction coordinate for ethylene hydrogenation to ethyl were observed to be fairly similar for the different pseudomorphic Pd/M(111) surfaces (Table 2). The C–H bond distances at the transition state are between 1.66 and 1.74 Å over the different Pd pseudomorphic overlayers. The C–Pd and H–Pd bond distances, however, are slightly longer on the Pd_{ML}/Re(0001) and Pd_{ML}/Ru(0001) overlayers as compared to those on Pd(111), consistent with the weaker interaction of the fragments with the bimetallic Pd_{ML}/Re(0001) and Pd_{ML}/Ru(0001) surfaces. The activation barriers and overall reaction energies for both ethylene hydrogenation and ethyldehydrogenation are shown in Table 2. The activation barriers for ethylene hydrogenation on Pd_{ML}/Re(0001), Pd_{ML}/Ru(0001), and Pd(111) are fairly similar (ca. 80 kJ/mol).

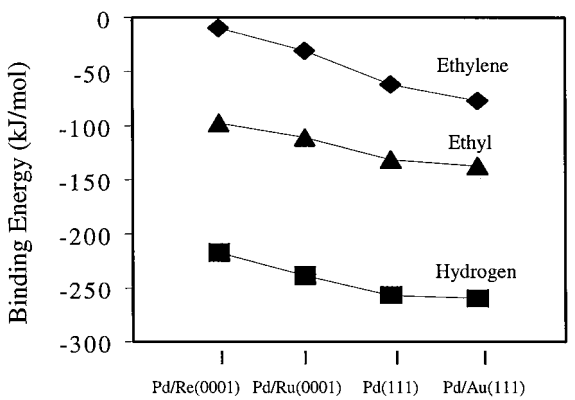

FIG. 5. DFT-computed binding energies of ethylene (◆), ethyl (▲), and atomic hydrogen (■) on Pd_{ML}/Re(0001), Pd_{ML}/Ru(0001), Pd(111), and Pd_{ML}/Au(111) surfaces.

The activation barrier for hydrogenation is about 20 kJ/mol higher on the Pd_{ML}/Au(111) surface. The reverse step, i.e., ethyl C–H bond activation, however, shows a more systematic trend in the activation energy. This barrier is highest on the Pd_{ML}/Re(0001) surface (ca. +126 kJ/mol) and lowest on the Pd_{ML}/Au(111) surface (ca. +72 kJ/mol). The DFT-computed activation barrier for C–H bond activation of ethyl to ethylene on Pd(111) (+82 kJ/mol) is slightly higher than the experimental estimate for ethyl C–H bond activation on Pd(100) (40–62 kJ/mol) (40). The barrier measured on the Pd(100) surface is most likely lower because it is more coordinatively unsaturated than the close-packed Pd(111) surface.

The structural features related to the reaction pathway are similar on the different pseudomorphic overlayers that were examined. This is an ideal situation for the development of structure–reactivity relationships. The changes in surface reactivity may be correlated either to changes in the overall thermodynamics for the reaction, such as the development of the Evans–Polanyi relationship, and/or to changes in the metal surface electronic structure. We examine both types of relationships. We first examine the results along the lines of energy differences. In the analysis section, we probe the correlation of activation energies with the electronic structure of the metal surface.

Linear free energy relationships. Based on empirical observation, Evans and Polanyi postulated that the activation energies for a series of reactions with structurally similar reactants are likely to correlate to the overall energies of reaction (81). This postulate is analogous to the Brønsted relation and is one of a series of linear free energy relationships (LFER) that correlate reaction rate constants to overall free energies of reaction. Another well-known concept in organic chemistry relates to the Hammond postulate, which states that for highly exothermic reactions the transition state structure and energy are similar to those of the reactant state (82). Conversely, for endothermic reactions, the transition state geometry and energy should be more product-like. While there is no rigorous foundation

$$\Delta E_a^i \propto \Delta(\Delta H_{rxn}^i)$$

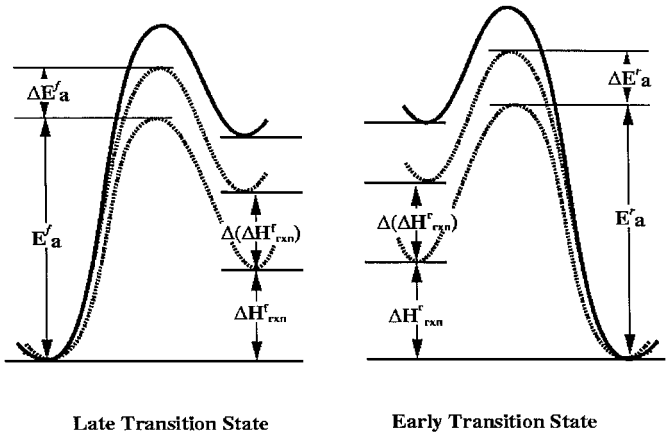

SCHEME 1

in theory, the Hammond postulate has held in the analysis of a fair number of experimental systems. The Hammond postulate suggests that, for reactions where the transition state is more product-like, the *forward* activation barrier should correlate to the overall forward energy of reaction. Analogously, for reactions with an early transition state, the activation barrier for the *reverse* reaction should correlate with the overall energy. This is illustrated in Scheme 1.

The results of plotting the forward activation barrier (for C–H bond formation) and the reverse activation barrier (for β-hydride elimination) as a function of the overall energy for hydrogenation of ethylene, on different metal surfaces, are shown in Figs. 6a and 6b, respectively. Figures 6a and 6b show that there is a near linear dependence between the activation barrier and the overall energy of reaction, consistent with expectations based on the Evans–Polanyi postulate. The activation barrier for β-hydride elimination of surface ethyl to ethylene is lower on surfaces where the overall energy for β-hydride elimination is more exothermic. Similarly, the activation barrier for ethylene hydrogenation to ethyl is lower on the surfaces, where the hydrogenation reaction is more exothermic. The slope for the activation barrier as a function of the overall energy for β-hydride elimination of ethyl is 0.65, which is within the range ($0 < \text{slope} < 1$) expected on the basis of the Evans–Polanyi postulate (83).

From Fig. 6, it is observed that the linear relationship between the activation barrier and the overall reaction energy is slightly better for β-hydride elimination as opposed to ethylene hydrogenation. This is rationalized on the basis of the reaction pathway for ethyl β-hydride elimination (see Fig. 1). The transition state (TS) is *late* along the reaction coordinate for β-hydride elimination of ethyl. The C–H bond distance of 1.7 Å at the transition state is significantly longer than that in the reactant ethyl species (1.1 Å) (Fig. 1). In other words, the transition state for β-hydride elimination of ethyl is structurally more product-like than reactant-like. Therefore, the stabilization of the transition state for β-hydride elimination on the different surfaces should be analogous to that of the product state. One would therefore expect a stronger dependence of the activation barrier for β-hydride elimination on the reaction energy, as compared to the activation barrier for C–H bond formation on the reaction energy. Our results are consistent with this expectation.

Figure 7 shows the activation barrier for ethylene hydrogenation and ethyl β C–H bond activation as a function of the ethylene adsorption energy on the surface. Earlier, we indicated that the trends in the overall energy for ethylene hydrogenation are very similar to those of ethylene adsorption. Figure 7 suggests that ethylene hydrogenation is slightly more favorable on surfaces where both ethylene and hydrogen are relatively weakly bound. The correlation of the activation barrier with the energy of adsorption of ethylene, however, is better for the reverse reaction of C–H bond breaking. The reverse C–H bond-breaking reaction appears to be more facile on surfaces where the dissociation

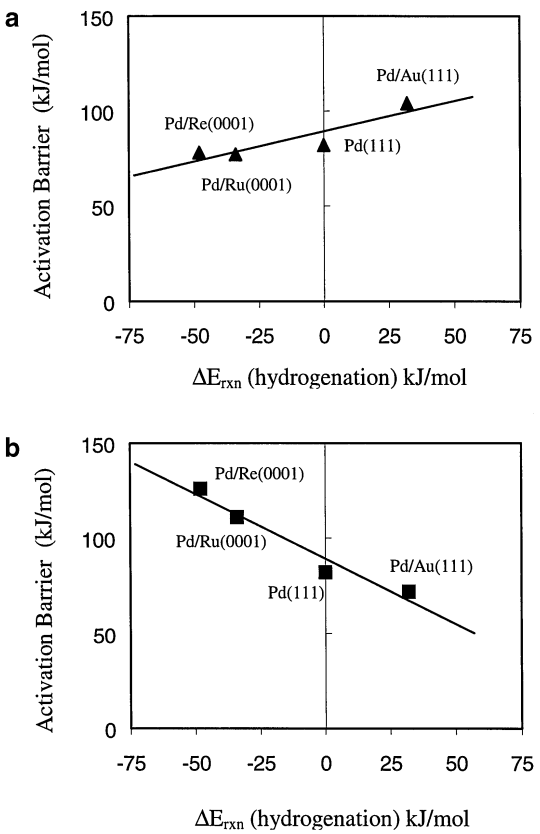

FIG. 6. Evans–Polanyi relationship for ethylene hydrogenation over pseudomorphic monolayers of Pd on Re, Ru, Pd, and Au. (a) DFT-GGA-calculated activation barrier for ethylene C–H bond formation versus ΔE_{rxn} for hydrogenation; (b) DFT-GGA- calculated activation barrier for ethyl C–H bond breaking versus ΔE_{rxn} for hydrogenation.

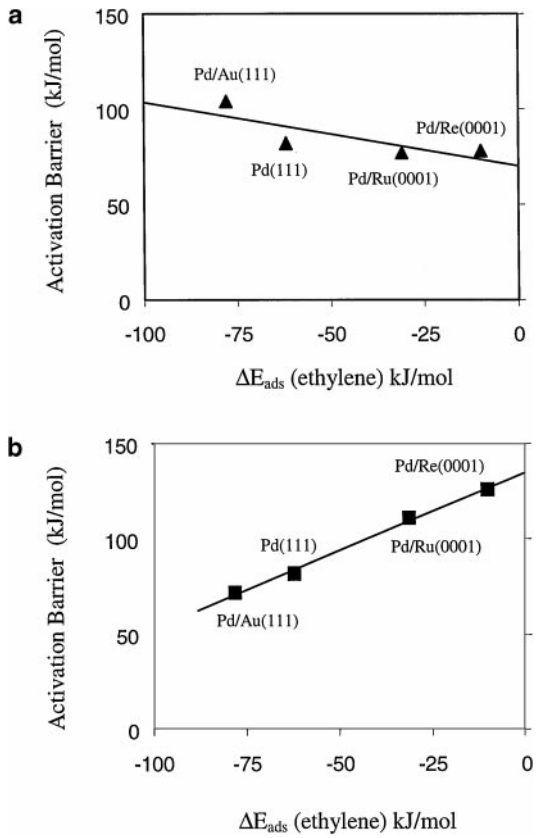

FIG. 7. DFT-calculated activation barrier for (a) ethylene hydrogenation and (b) ethyl C–H bond breaking, as a function of ethylene adsorption energy on pseudomorphic Pd overlayers.

products, i.e., ethylene and hydrogen, are more strongly bound. This is not an unexpected result. Hydrogenation of ethylene to ethyl involves the breaking of metal–adsorbate bonds and the formation of adsorbate–adsorbate bonds. One would therefore expect it to be easier to combine fragments on surfaces that have relatively weaker metal–adsorbate bond strengths. The DFT results appear to conform to this expectation, based on the Sabatier principle.

3.3. Dehydrogenation of Di-σ-Bound Ethylene to Vinyl

To study the role of the metal in adsorbate bond breaking, the dehydrogenation of di-σ-bound ethylene to vinyl was examined for all the surfaces of interest in this paper. The DFT-computed reaction pathway for the formation of vinyl from ethylene was discussed in section 1.3. The DFT-optimized structures for the reactant, transition state, and product on Pd(111) are depicted in Fig. 3. The energetics for C–H bond activation of ethylene to vinyl on the different surfaces are tabulated in Table 3. The dehydrogenation of ethylene to vinyl at $(\sqrt{3} \times \sqrt{3})$ coverage is at least 70 kJ/mol endothermic for all the Pd-based surfaces studied here. The reaction is most endothermic on the Pd_{ML}/Re(0001) surface with a ΔE_{rxn} of +139 kJ/mol. In comparison, the

TABLE 3

Activation Barriers and Energy of Reaction for Ethylene Dehydrogenation to Vinyl on Pd(111) and Pseudomorphic Monolayers of Pd(111) on Re(0001), Ru(0001), and Au(111) ($C_2H_4^* + * \underset{k_r}{\overset{k_f}{\rightleftarrows}} C_2H_3^* + H^*$)

Surface	ΔE_{rxn} (kJ/mol) dehydrogenation	ΔE_{act}^{f} (kJ/mol) dehydrogenation	ΔE_{act}^{r} (kJ/mol) vinyl hydrogenation
Pd_{ML}/Re(0001)	+139	+188	+49
Pd_{ML}/Ru(0001)	+120	+172	+51
Pd(111)	+73	+151	+78
Pd_{ML}/Au(111)	+77	+143	+66

reaction is slightly more favorable on the Pd(111) and Pd_{ML}/Au(111) surfaces that have energies of reaction of +73 and +77 kJ/mol, respectively. The energy of reaction on the Pd_{ML}/Ru(0001) surface is +120 kJ/mol, which is intermediate to that on the Pd(111) and Pd_{ML}/Re(0001) surfaces.

The binding energies of atomic hydrogen, vinyl, and ethylene for the different pseudomorphic Pd overlayers are shown in Fig. 8. It is observed that the binding energy of all intermediates are stronger as we move from the Pd_{ML}/Re(0001) surface toward the Pd_{ML}/Au(111) surface. The graph also shows that there is a somewhat stronger variation in the vinyl binding energy as compared to the ethylene and hydrogen binding energies. One would therefore expect the overall reaction energy for vinyl formation to follow the changes in the vinyl binding energy.

Table 3 shows the DFT-computed forward and reverse activation barriers for ethylene C–H bond activation to vinyl. The results indicate that vinyl formation has an activation energy of +151 kJ/mol on the Pd(111) surface. The reaction is slightly favored on the Pd_{ML}/Au(111) surface, where the barrier is +143 kJ/mol. The dehydrogenation reaction has relatively higher activation barriers of +172 and +188 kJ/mol on the Pd_{ML}/Ru(0001) and Pd_{ML}/Re(0001)

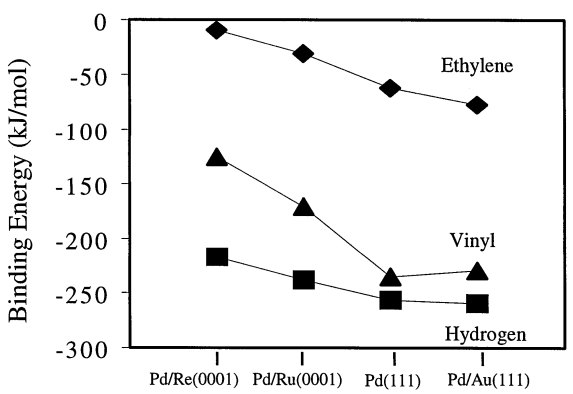

FIG. 8. DFT-computed binding energies of ethylene (◆), vinyl (▲), and atomic hydrogen (■) on Pd_{ML}/Re(0001), Pd_{ML}/Ru(0001), Pd(111), and Pd_{ML}/Au(111) surfaces.

surfaces, respectively. Experimental estimates of the activation barrier for vinyl formation are not available for the above-mentioned surfaces. However, Zaera and coworkers report that vinyl hydrogenation to ethylene occurs at about 200 K on Pt(111) (38). Based on this observation, the activation barrier for vinyl hydrogenation on Pt(111) is estimated to be about 40–50 kJ/mol. Our calculated value for vinyl hydrogenation on Pd(111) is 70 kJ/mol, which is about 20 kJ/mol higher than the estimated experimental activation energy on Pt(111).

Similar to the analysis for ethylene hydrogenation, the activation barriers for vinyl hydrogenation and ethylene C–H bond breaking are plotted as a function of the overall energy of reaction for ethylene dehydrogenation (Figs. 9a and 9b). This graph provides a test of the Evans–Polanyi postulate for this particular step. Again, we find that the activation barrier for C–H bond-breaking *decreases* as the energy of reaction for C–H bond activation becomes less *endothermic*. The activation barrier for the reverse step, vinyl hydrogenation to ethylene, also *decreases* as the reaction energy for hydrogenation becomes more *exothermic*.

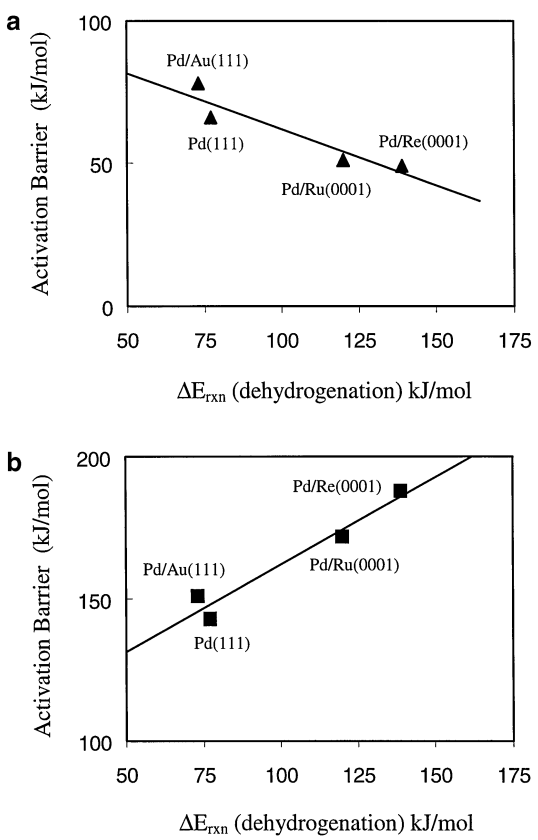

FIG. 9. Evans–Polanyi relationship for ethylene dehydrogenation over pseudomorphic monolayers of Pd on Re, Ru, Pd, and Au. (a) DFT-GGA calculated activation barrier for vinyl C–H bond formation versus ΔE_{rxn} for dehydrogenation; (b) DFT-GGA-calculated activation barrier for ethylene C–H bond breaking versus ΔE_{rxn} for dehydrogenation.

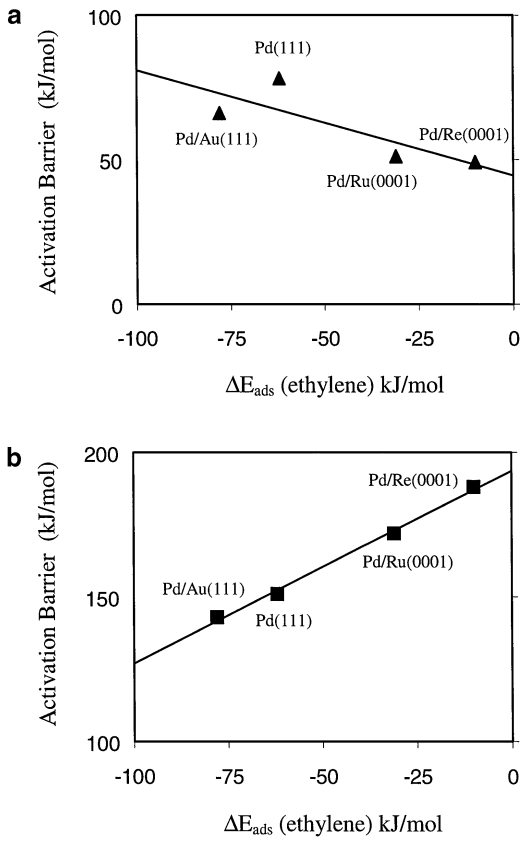

FIG. 10. DFT-calculated activation barrier for (a) vinyl hydrogenation and (b) ethylene C–H bond breaking, as a function of ethylene adsorption energy on pseudomorphic Pd overlayers.

Remarkably, the slope of the Evans–Polanyi plot for C–H bond activation of ethylene and ethyl are almost identical, with a value of 0.65. This is most likely because the reaction mechanism for C–H bond activation and the location of the transition state along the reaction coordinate for ethyl and ethylene are very similar.

Figure 10 shows the activation barrier for ethylene C–H bond activation as a function of the ethylene binding energy. The figure suggests that C–H bond activation of ethylene is easier on surfaces where ethylene is more strongly bound. Again, this is consistent with our expectation based on metal–adsorbate bond strengths. Since vinyl formation results in more metal–adsorbate bonds than the reactant (di-σ-bound ethylene), surfaces that form stronger metal–adsorbate bonds appear to favor C–H bond breaking of ethylene.

4. ANALYSIS

4.1. Electronic Factors Determining Ethylene Adsorption and Reaction Energetics on $Pd_{ML}/M(111)$ (M = Re, Ru, Pd, and Au) Surfaces

In the results presented so far, we have shown that ethylene and hydrogen are very weakly bound to the

Pd_{ML}/Re(0001) surface and strongly bound to the Pd_{ML}/Au(111) surface. This result is somewhat surprising since it seems to suggest that Pd_{ML}/Re(0001) is relatively inert for ethylene and hydrogen adsorption as compared to both Pd(111) and Re(0001) surfaces. In contrast, the Pd_{ML}/Au(111) surface appears to be more reactive than both the Pd(111) and Au(111) surfaces for ethylene and hydrogen adsorption. In the following section, we analyze the adsorption characteristics of the surface based on the changes in the electronic properties of the metal surface layer, in an attempt to explain the nonlinearity in the adsorption strengths on bimetallic pseudomorphic overlayers.

In section 3.2 we showed that the hydrogenation of ethylene has a lower barrier on the surfaces to which ethylene and hydrogen are weakly bound. Conversely, the dehydrogenation of ethylene to surface vinyl showed the opposite trend; i.e., the dehydrogenation reaction was more favorable on surfaces where ethylene, vinyl, and hydrogen were more strongly adsorbed (section 3.3). From a catalysis perspective, it would be interesting to examine how structural and electronic changes of the metal surface affect the activation barriers for these two opposite reactions, hydrogenation and dehydrogenation.

In the reactions studied in this paper, the elementary C–H bond breaking (vinyl formation) or C–H bond formation (ethyl formation) processes take place over the Pd overlayer atoms, without *direct* participation by the substrate metal. However, from the results presented in this paper, it is evident that the metal substrate plays an important role in perturbing the electronic structure and chemical reactivity of the surface Pd atoms. In the remaining sections, we will analyze the intrinsic electronic properties of the surface that influence surface reactivity. The DFT-predicted trends are rationalized on the basis of a simplified model from formal chemisorption theory that was proposed by Hammer and Nørskov (69, 79, 80, 84). The Hammer–Nørskov model is an extension of the Newns–Anderson chemisorption model (2, 69, 85–87).

4.2. Adsorption of Ethylene on Pd(111) and Bimetallic Pd(111)/M(111) (M = Re, Ru, and Au)

The di-σ adsorption of ethylene on a metal surface involves the interaction of the frontier π- (HOMO) and π*- (LUMO) orbitals of ethylene with the s-, p-, and d-band of the metal. Figure 11 shows the π- and π*-orbitals of vapor-phase ethylene (see lowermost frame of Fig. 11). Following the Hammer–Nørskov procedure (69), the interaction of the π- and π*-states with the valence sp-band of transition metals was determined by performing DFT calculations for ethylene on Al(111). The interaction of the π- and π*-orbitals with the sp-band results in a broadening and slight downshift of the frontier orbital states of ethylene. The renormalized π*-state is located very close to the Fermi energy, while the renormalized π-state is located about

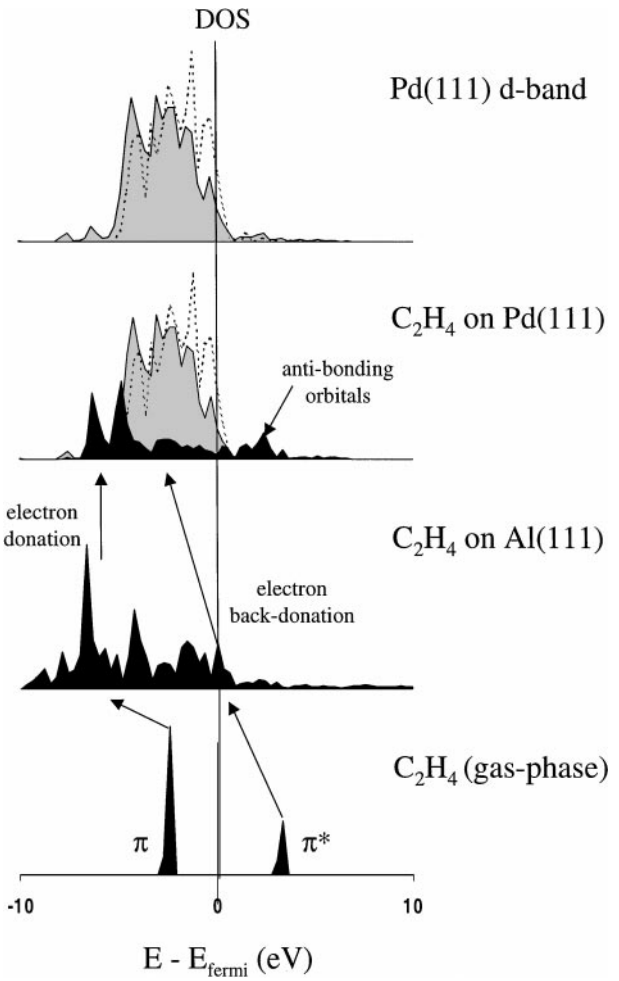

FIG. 11. Frontier orbital interactions in the di-σ adsorption of ethylene on Pd(111). Dark shaded regions indicate density of states (DOS) projected to the carbon 2*p* orbital state. Lightly shaded areas correspond to DOS projected to the surface Pd d-band. The bare Pd(111) surface d-band (dotted line) is shown for comparison.

6.0 eV below the Fermi energy. The renormalized π- and π*- states also couple with the valence d-band of the metal, resulting in bonding and antibonding overlap orbitals. Since the π*-state is closest to the Fermi energy, the coupling of the π*-state of ethylene with the metal d-band is stronger than the interaction of the π-orbital with the d-band.

Following the procedure of Hammer and Nørskov, the interaction energy of ethylene with a metal surface may be approximated by the expression (69)

$$E_{ads} = E_{sp} + E_{d\text{-}hyb}, \qquad [1]$$

where E_{sp} is the contribution to the total chemisorption energy (E_{ads}) of the interaction of ethylene with the sp-band of the metal. $E_{d\text{-}hyb}$ is the contribution due to the interaction of ethylene with the valence d-band. As an approximation, the $E_{d\text{-}hyb}$ term may be written in terms of coupling of the

renormalized π- and π*-states of ethylene with the d-band.

$$E_{\text{d-hyb}} \approx -2 \cdot \left[f \frac{V_{\pi^*}^2}{\varepsilon_{\pi^*} - \varepsilon_d} + f \cdot S_{\pi^*} V_{\pi^*} \right] - 2 \cdot \left[(1 - f) \frac{V_{\pi}^2}{\varepsilon_d - \varepsilon_{\pi}} + (1 + f) \cdot S_{\pi} V_{\pi} \right], \quad [2]$$

where f is the d-band filling, V_{π}^2 and $V_{\pi^*}^2$ are the d-band coupling matrix elements for interaction with the renormalized π- and π*-states, respectively, S_{π} and S_{π^*} are overlap matrix elements related to the coupling elements V by the expression $S = -\alpha V$ (α is a constant for the metal–adsorbate system), ε_{d} is the location of the metal d-band center relative to the Fermi-energy, and ε_{π} and ε_{π^*} are the renormalized energies of the π- and π*-orbitals of ethylene, with respect to the Fermi energy, after interaction with the sp-band.

The first term of Eq. [2] corresponds to the hybridization gain and orthogonalization cost associated with the interaction of the π*-state of ethylene with the metal d-band. In frontier orbital theory, this term is referred to as *electron backdonation*. The second term of Eq. [2] is the hybridization gain and orthogonalization cost related to the interaction of the π-orbital of ethylene with the metal d-band. This interaction is traditionally referred to as *electron donation*.

Figure 12 shows the valence sp- and d-bands projected to the surface Pd layer for all the surfaces examined in this paper. It is observed that the sp-band projected to the surface Pd atoms is broad, diffuse, and almost identical for all the surfaces. It is therefore reasonable to assume that the interaction energy of ethylene with the sp-band is almost the same for the surfaces of interest here (69). There are noticeable differences, however, in the d-band projected to the Pd overlayer. The projected d-band is located between +0.5 and −5.0 eV of the Fermi energy for the different surfaces (Fig. 12). However, as the substrate is changed from Re to Au, the fraction of the d-band which is close to the Fermi level increases substantially. Table 4 summarizes the electronic properties for the bare metal surfaces. The d-band filling for the surface Pd layer is determined by integrating the area under the projected d-band from $-\infty$ to $+\infty$ and calculating the fractional area that is located below the Fermi energy. Table 4 shows that there are negligible differences in the d-band filling for the surface Pd atoms as the substrate is changed from Re to Au. The Pd d-band filling is approximately 0.96 for all the surfaces studied here.

The d-band center for the Pd overlayer was calculated by taking the first moment of the projected density of d-states about the Fermi energy. The d-band center of monometallic Pd(111) is located 2.0 eV below the Fermi energy. When the substrate is a metal such as Re or Ru that is to the left of Pd in the periodic table, the d-band center shifts farther away from the Fermi energy. On the other hand, a pseudomorphic overlayer of Pd on a noble metal such as Au has a d-band center which has moved closer to the Fermi

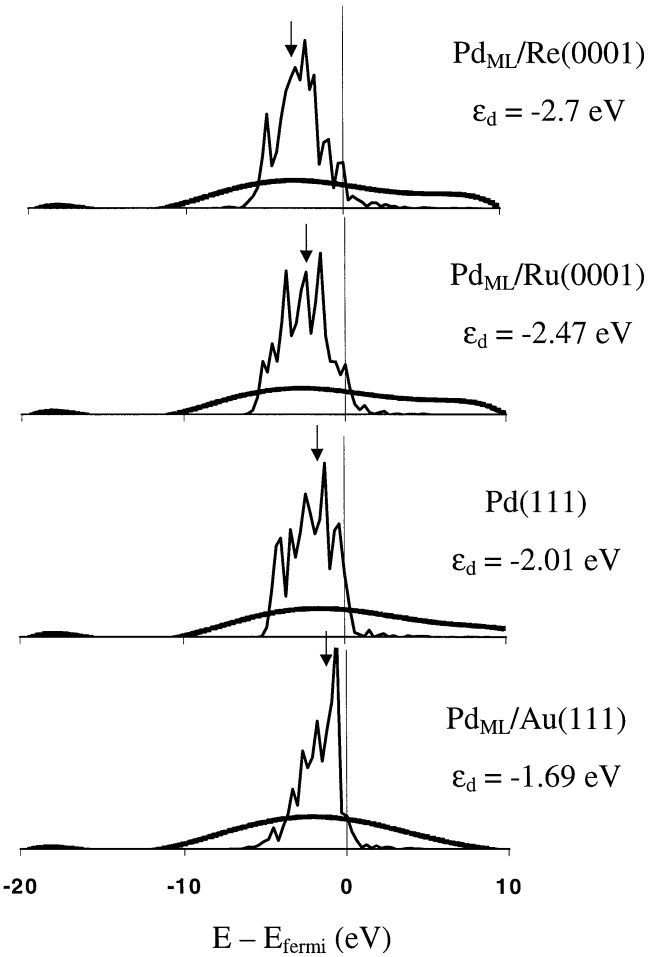

FIG. 12. Electronic density of states (DOS) projected to the surface Pd layer of pseudomorphic Pd$_{ML}$/Re(0001), Pd$_{ML}$/Ru(0001), Pd(111), and Pd$_{ML}$/Au(111) surfaces. Thin line indicates projection to the valence d-band. Thicker line corresponds to the sp-band. Arrow indicates location of d-band centers (ε_{d}).

level. Ruban *et al.* have compiled an extensive database of d-band center shifts for pseudomorphic overlayers of one transition metal over another using linearized muffin tin orbital (LMTO) calculations (22, 69). The shifts in the d-band centers reported here are consistent with Ruban *et al.*'s

TABLE 4

Surface Electronic Properties of Bare Pd$_{ML}$/Re(0001), Pd$_{ML}$/Ru(0001), Pd(111), and Pd$_{ML}$/Au(111) Slabs

Surface	d-Band coupling element[a] V^2 (eV)^2	d-Band filling[a] f	d-Band center[a] ε_{d} (eV)	Work function (eV)
Pd$_{ML}$/Re(0001)	2.78	0.9601	−2.7	5.00
Pd$_{ML}$/Ru(0001)	2.78	0.9566	−2.47	5.09
Pd(111)	2.78	0.9621	−2.01	5.30
Pd$_{ML}$/Au(111)	2.78	0.9623	−1.69	5.36

[a] Indicated electronic properties are for the surface Pd layer.

calculated values. Koel and co-workers have experimentally determined that the valence d-band of $Pd_{ML}/Au(111)$ is located about 1.6 eV below the Fermi level (9). Our computed value of 1.69 eV is in excellent agreement with their experimental measurement.

The projected d-band centers for the surface Pd layer over different substrates are located between −1.5 and −2.7 eV of the Fermi energy. Earlier, we said that the renormalized π- and π*-states of ethylene after interaction with the sp-band are situated approximately −6.0 and 0 eV, respectively, relative to the Fermi energy. This implies that the d-band center is in better resonance with the π*-state than with the π-orbital of ethylene. Coupled with the fact that the d-band filling (f) for all the surfaces is close to unity, Eq. [2] may be simplified to

$$E_{\text{d-hyb}} \approx -2 \cdot \left[f \frac{V_{\pi^*}^2}{\varepsilon_{\pi^*} - \varepsilon_d} + f \cdot S_{\pi^*} V_{\pi^*} + (1 + f) \cdot S_{\pi} V_{\pi} \right]. \quad [3]$$

The d-band coupling element is an intrinsic property of the surface metal atom and is assumed to be independent of the substrate. If we further assume that the orthogonalization cost is roughly the same for all the surfaces examined here, in the perturbation limit, Eq. [3] may be rewritten as

$$\delta E_{\text{d-hyb}} \approx -2 \cdot \left[f \frac{V_{\pi^*}^2}{(\varepsilon_{\pi^*} - \varepsilon_d)^2} \right] \cdot \delta\varepsilon_d, \quad [4]$$

where $\delta E_{\text{d-hyb}}$ is the change in the adsorption energy of ethylene due to the $\delta\varepsilon_{\text{d}}$ shift in the surface d-band center. Equation [4] is very similar to the analysis of Hammer and Nørskov for CO adsorption on metal surfaces (84). Equation [4] predicts that changes in the adsorption energy of ethylene should correlate linearly with shifts in the surface metal d-band center. In Fig. 13, we have plotted the di-σ adsorption energy of ethylene as a function of the surface metal d-band center. The plot shows a near linear correlation between the ethylene adsorption energy and the bare surface d-band center, confirming the predictions based on the Hammer–Nørskov model. Figure 13 shows that ethylene binding energies are higher on pseudomorphic Pd overlayer surfaces, where the Pd d-band center is closer to the Fermi energy. The weaker ethylene adsorption energy for Pd monolayers on Re(0001) and Ru(0001) are due to the weaker backdonation interaction between the surface Pd d-band and the ethylene π*-orbital. In analyzing the adsorption of ethylene on $Pd_{ML}/Mo(100)$, Koel and co-workers argued that the weaker adsorption of ethylene on the $Pd_{ML}/Mo(100)$ surface, relative to Pd(111), was due to rehybridization of the Pd d-band to lower energies, causing decreased backdonation to the ethylene π*-orbital (68). Our theoretical calculations are consistent with the speculations of Koel and co-workers.

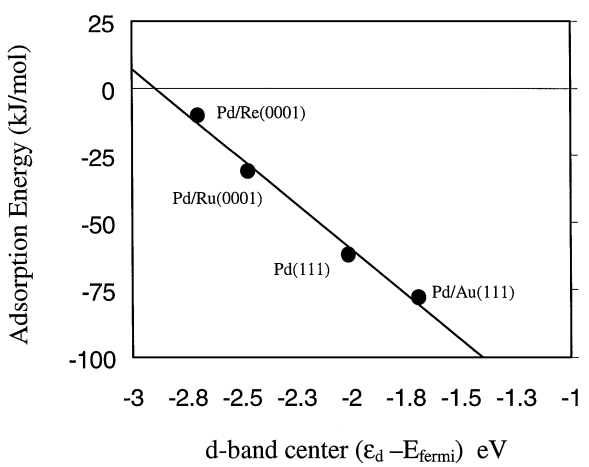

FIG. 13. DFT-GGA-predicted ethylene adsorption energy as a function of the Pd d-band center of the bare metal surfaces of $Pd_{ML}/Re(0001)$, $Pd_{ML}/Ru(0001)$, Pd(111), and $Pd_{ML}/Au(111)$.

4.3. C–H Bond Activation of Ethyl and Ethylene on Pd(111) and Bimetallic Pd(111)/M(111) (M = Re, Ru, and Au) Surfaces

In the previous section, we showed how the Hammer–Nørskov analysis allows the correlation of the ethylene di-σ adsorption energy to an intrinsic electronic property of the bare metal surface. In this section, the analysis is extended to the correlation of activation barriers for the hydrogenation/dehydrogenation of ethylene to the bare surface electronic properties.

Although the transition state is a short-lived species, the electronic interactions of the transition state with a metal surface are not fundamentally different from the interactions of molecular and atomic adsorbates with metals. The coupling of the transition state to the metal is often controlled by electron donation and backdonation interactions with the metal surface. Since the Hammer–Nørskov analysis correlates metal–adsorbate binding strengths to frontier orbital interactions, it is easily extended to the analysis of transition states. To accomplish this, Hammer and Nørskov introduced an approximate reactivity measure to examine trends in the activation barrier for H_2 adsorption on metals (69, 80). This reactivity measure is based on estimating the strength of interaction between the adsorbate and the metal, at the transition state.

In section 1.2, we analyzed the electronic interactions between the transition state and the metal for ethyl C–H bond activation. By following Hammer and Nørskov's analysis (80), we can approximate the interaction energy (δE_{ts}) at the transition state for ethyl and ethylene C–H bond breaking by the expression

$$\delta E_{\text{ts}} = -2 \cdot \left[f \frac{V_{\sigma_{\text{CH}^*}}^2}{\varepsilon_{\sigma_{\text{CH}^*}} - \varepsilon_d} + f \cdot S_{\sigma_{\text{CH}^*}} V_{\sigma_{\text{CH}^*}} \right] - 2 \cdot \left[(1 - f) \frac{V_{\sigma_{\text{CH}}}^2}{\varepsilon_d - \varepsilon_{\sigma_{\text{CH}}}} + (1 + f) \cdot S_{\sigma_{\text{CH}}} V_{\sigma_{\text{CH}}} \right]. \quad [5]$$

This expression is very similar to the one written earlier for adsorption (i.e., Eq. [2]), except that the frontier orbitals of interest, at the transition state, are the σ_{CH} and σ_{CH^*} orbitals. Since the d-band of the Pd overlayer is in better resonance with the antibonding σ_{CH^*} state and the d-band filling for the surface Pd layer in all cases is close to unity, we can simplify Eq. [5] to

$$\delta E_{ts} = -2 \cdot \left[f \frac{V^2_{\sigma_{CH^*}}}{\varepsilon_{\sigma_{CH^*}} - \varepsilon_d} + f \cdot S_{\sigma_{CH^*}} V_{\sigma_{CH^*}} + (1 + f) \cdot S_{\sigma_{CH}} V_{\sigma_{CH}} \right]. \quad [6]$$

If we assume that the orthogonalization cost is nearly the same for all the surfaces studied here, as an approximation, the shift in the interaction energy at the transition state can be correlated to the d-band center through the expression

$$\Delta\delta E_{ts} = -2 \cdot \left[f \frac{V^2_{\sigma_{CH^*}}}{\left(\varepsilon_{\sigma_{CH^*}} - \varepsilon_d\right)^2} \right] \cdot \Delta\varepsilon_d. \quad [7]$$

If it is further assumed that the activation barriers are in some respect proportional to the reactivity measure, a linear correlation would be expected between the activation barrier and the d-band center of the pseudomorphic Pd overlayer. In Fig. 14, we have tested the model by plotting the DFT-computed ethyl and ethylene C–H bond activation barrier as a function of the bare metal d-band center. The excellent correlation between these two parameters demonstrates the effectiveness of the Hammer–Nørskov analysis for correlating the activation barrier to an intrinsic surface electronic property (i.e., the d-band center). Figure 14 shows that the C–H bond activation barriers for ethyl and ethylene decrease as the surface Pd d-band center shifts closer toward the Fermi energy. This is because the C–H bond activation process on these surfaces is primarily controlled by backdonation into the σ_{CH^*} orbital and is more favored as the d-band of the metal is in resonance with this antibonding state.

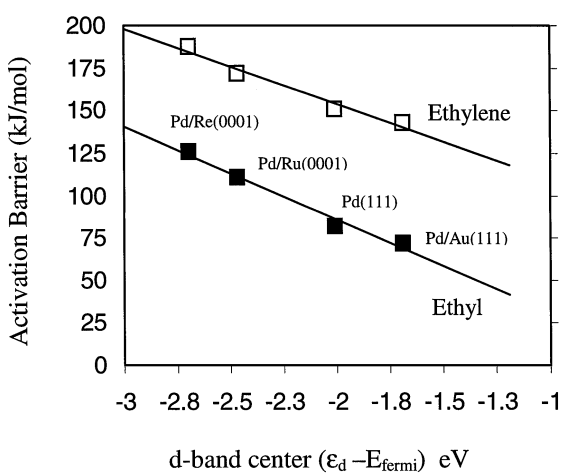

FIG. 14. DFT-GGA-computed C–H bond activation barriers for ethylene (❑) and ethyl (■) versus the Pd d-band center of the bare metal surfaces of Pd_{ML}/Re(0001), Pd_{ML}/Ru(0001), Pd(111), and Pd_{ML}/Au(111).

An interesting observation from Fig. 14 is that the slopes of the C–H bond activation barrier as a function of the d-band center are almost identical for ethyl and ethylene. The results we present here are actually an extension of the ideas originally introduced by Hammett in analyzing the electronic effect of substituents ($-X$) on the reactivity of substituted benzenes (88). Hammett's equation is traditionally written as (89)

$$\log_{10}\left(\frac{k_x}{k_0}\right) = \rho\sigma, \quad [7]$$

where the ratio (k_x/k_0) is the enhancement in the reaction rate due to the presence of the substituent (X), in comparison to a homologous reference molecule. σ is some measure of the electron-withdrawing nature of the substituent X. ρ is the measure of the influence of the electron-withdrawing substituent (X) on the reaction rate (89). Hammett suggested that if a linear correlation is obtained for $\log_{10}(k_x/k_0)$ plotted as a function of the σ parameter, it implies that the position of the transition state is not changing as a result of changing the substituent and that the reaction mechanism is invariant (89). In our work, the d-band center is somewhat analogous to the σ parameter because it is a measure of the electron-backdonating capability of the metal surface to the reacting entity. Since the C–H bond activation mechanism remains the same, the linearity in the activation barrier vs the d-band center should be preserved. A close comparison of the slopes for C–H bond activation of ethyl and ethylene as a function of the d-band center (Fig. 14) demonstrates that the electronic influence of the metal surface on C–H bond breaking is very similar in both cases. In analogy to Hammett's equation, this is tantamount to having an identical "ρ" parameter for ethylene and ethyl C–H bond activation on the various pseudomorphic Pd overlayers. The changes in the intercept as one changes the reactant should correlate with the electronic properties of the reactant. Developing such correlations could have an important impact on the design of new systems, whereby the electronic structure of the surface and the reactant could be easily computed independently to tailor optimal reactant–substrate reactivity.

5. CONCLUSIONS

The ($\sqrt{3} \times \sqrt{3}$) periodic adsorption of ethylene was examined on pseudomorphic overlayers of Pd on Re(0001), Ru(0001), Pd(111), and Au(111) substrates, using DFT-GGA slab calculations. The adsorption energies for ethylene on Pd_{ML}/Re(0001), Pd_{ML}/Ru(0001), Pd(111), and Pd_{ML}/Au(111) were estimated to be −10, −31, −62, and

−78 kJ/mol, respectively. The DFT-computed dissociative adsorption energies for H_2 on these surfaces were +2, −6, −78, and −83 kJ/mol, respectively, for 100% surface coverage on each surface. The calculated trends in adsorption energies are in good agreement with experimental observations for adsorption of CO on the pseudomorphic overlayers (7, 9). The weaker adsorption energy for ethylene on Pd_{ML}/Re(0001) and Pd_{ML}/Ru(0001), relative to Pd(111), is because of the weaker backdonation interaction between the metal d-band and the ethylene π*-orbital. This is identical to the arguments used by Koel and co-workers to explain the weaker adsorption strengths of ethylene on Pd_{ML}/Mo(100) as compared to those on Pd(111) (68).

In addition to chemisorption, the surface reactions of ethylene hydrogenation to ethyl and ethylene dehydrogenation to vinyl were examined on all the surfaces. Based on the DFT-computed results, it appears that the hydrogenation of ethylene to ethyl and the hydrogenation of vinyl to ethylene have lower activation barriers on surfaces to which the adsorbates are weakly bound. The activation barrier for hydrogenation is, therefore, low on the Pd_{ML}/Re(0001) surface and high on the Pd_{ML}/Au(111) surface. On the other hand, dehydrogenation reactions of ethyl and ethylene are favored on surfaces with stronger metal–adsorbate bond strengths. β-Hydride elimination of ethyl and vinyl formation have lower activation barriers on Pd_{ML}/Au(111) as compared to Pd_{ML}/Re(0001). In all cases, the activation barriers are observed to correlate linearly with the overall reaction energy, consistent with the Evans–Polanyi relationship and the Hammond postulate. The correlation between the C–H bond activation barrier and overall reaction energy is most evident for the β-hydride elimination of both ethyl and ethylene, which have slopes of 0.65. This is within the range ($0 < \text{slope} < 1$) expected on the basis of the Evans–Polanyi postulate. The identical slopes for ethyl and ethylene C–H bond activation on the Evans–Polanyi plot are likely because of the very similar mechanism for both reactions and the analogous location of the transition state along the reaction coordinate.

Finally, we have analyzed the DFT-predicted trends in ethylene adsorption energy and the activation barriers for hydrogenation/dehydrogenation based on frontier-orbital theory and the Hammer–Nørskov model (2, 69, 87, 90, 91). It appears that the d-band center of the surface metal atom is an important parameter that helps to determine the strength of adsorption of ethylene and hydrogen on the surface. Ethylene and hydrogen are more strongly bound on surfaces where the d-band center is closer to the Fermi level. Activation barriers for C–H bond breaking of ethyl and ethylene also appear to correlate to the surface Pd d-band center. The C–H bond activation process is primarily governed by the backdonation of electrons from the metal into the antibonding σ*-orbital of the adsorbate. Surfaces where the d-band center is closer to the Fermi energy are therefore more reactive for dehydrogenation. The Pd_{ML}/Au(111) surface, which has the d-band center closest to the Fermi level, amongst all the surfaces examined here, has the lowest barrier for C–H bond breaking. On the other hand, the Pd_{ML}/Re(0001) surface, which has the d-band center farthest from the Fermi level, favors ethylene hydrogenation. The trends are consistent with the ideas of Hammett which suggest that the slope of the correlation will hold for other molecules, provided that the mechanism remains the same.

ACKNOWLEDGMENTS

We would like to thank Professor Jens Nørskov, Professor Bjørk Hammer, and Dr. Lars Hansen for helpful discussions as well as for the use of their plane-wave pseudopotential program. We also thank Dr. Victor S. Lusvardi, Dr. Kathy Saturday, Dr. Jan Lerou, Dr. Bruce Smart, and Professor Robert J. Davis for their helpful discussions. The DuPont Chemical Company (USA) and the NSF (Career Award CTS-9702762) are acknowledged for financial support. Acknowledgment is made to the donors of The Petroleum Research Fund (Grant 31342G5), administered by the ACS, for support of this research. V.P. expresses gratitude to the University of Minnesotta-IBM Shared Research Project, ACS, and the NSF (CDA-9502979) for support through the IBM Graduate Student Award in Computational Chemistry.

REFERENCES

1. Masel, R. I., "Principles of Adsorption and Reaction on Solid Surfaces." John Wiley and Sons, Inc., New York, 1996.
2. van Santen, R. A., "Theoretical Heterogeneous Catalysis." World Scientific Publishing Company, Pvt. Ltd., Singapore, 1991.
3. Sinfelt, J. H., "Bimetallic Catalysts: Discoveries, Concepts and Applications." Wiley, New York, 1983.
4. Schwartz, J. T., E. I. DuPont de Nemours and Company, U.S. Patent 5,478,952, 1995.
5. Mabry, M., Prichard, W., and Ziemecki, S., E. I. DuPont de Nemours and Company, U.S. Patent 4,609,636, 1986.
6. Mabry, M., Prichard, W., and Ziemecki, S., E. I. DuPont de Nemours and Company, U.S. Patent 4,550,185, 1985.
7. Campbell, R. A., Rodriguez, J. A., and Goodman, D. W., *Phys. Rev. B* **46**, 7077 (1992).
8. Rodriguez, J. A., and Goodman, D. W., *Science* **257**, 897 (1992).
9. Sellidj, A., and Koel, B. E., *Phys. Rev. B* **49**, 8367 (1994).
10. Koel, B. E., Sellidj, A., and Paffett, M. T., *Phys. Rev. B* **46**, 7846 (1992).
11. Xinyin, S., Frankel, D. J., Hermanson, J. C., Lapeyre, G. J., and Smith, R. J., *Phys. Rev. B* **32**, 2120 (1985).
12. Hasegawa, Y., Jia, J. F., Inoue, K., Sakai, A., and Sakurai, T., *Surf. Sci.* **386**, 328 (1997).
13. Baddeley, C. J., Barnes, C. J., Wander, A., Ormerod, R. M., King, D. A., and Lambert, R. M., *Surf. Sci.* **314**, 1 (1994).
14. Bauer, E., *in* "The Chemical Physics of Solid Interfaces and Heterogeneous Catalysis" (D. A. King and D. P. Woodruff, Eds.), Vol. 3. Elsevier, Amsterdam, 1984.
15. Rodriguez, J. A., and Goodman, D. W., *J. Phys. Chem.* **95**, 4196 (1991).
16. Campbell, C. T., *Annu. Rev. Phys. Chem.* **41**, 775 (1990).
17. Godbey, D. J., and Somorjai, G. A., *Surf. Sci.* **204**, 301 (1988).
18. Santra, A. K., and Rao, C. N. R., *Appl. Surf. Sci.* **84**, 347 (1995).
19. Pick, S., *J. Phys. Chem.* **99**, 15375 (1995).
20. Wu, R., and Freeman, A. J., *Phys. Rev. B* **52**, 12419 (1995).

21. Hammer, B., Morikawa, Y., and Nørskov, J. K., *Phys. Rev. Lett.* **76**, 2141 (1996).
22. Ruban, A., Hammer, B., Stoltze, P., Skriver, H. L., and Nørskov, J. K., *J. Mol. Catal. A: Chem.* **115**, 421 (1997).
23. Pallassana, V., Neurock, M., Hansen, L., Hammer, B., and Nørskov, J., *Phys. Rev. B* **60**, 6146 (1999).
24. Pallassana, V., Neurock, M., and Coulston, G. W., *J. Phys. Chem. B* **103**(42), 8973 (1999).
25. Stuve, E. M., and Madix, R. J., *J. Phys. Chem.* **89**, 105 (1985).
26. Guo, X., and Madix, R. J., *J. Catal.* **155**, 336 (1995).
27. Gates, J. A., and Kesmodel, L. L., *Surf. Sci.* **120**, L461 (1982).
28. Ratajczykowa, I., and Szymerska, I., *Chem. Phys. Lett.* **96**, 243 (1983).
29. Sekitani, T., Takaoka, T., Fujisawa, M., and Nishijima, M., *J. Phys. Chem.* **96**, 8462 (1992).
30. Nishijima, M., Yoshinobu, J., Sekitani, T., and Onchi, M., *J. Chem. Phys.* **90**, 5114 (1989).
31. Merrill, P. B., and Madix, R. J., *J. Am. Chem. Soc.* **118**, 5062 (1996).
32. Cremer, P. S., Su, X., Shen, Y. R., and Somorjai, G. A., *J. Am. Chem. Soc.* **118**, 2942 (1996).
33. Zaera, F., *Langmuir* **12**, 88 (1996).
34. Windham, R. G., Koel, B. E., and Paffett, M. T., *Langmuir* **4**, 1113 (1988).
35. White, J. M., *Langmuir* **10**, 3946 (1994).
36. Borg, H. J., van Hardeveld, R. M., and Niemantsverdriet, J. W., *J. Chem. Soc. Faraday Trans.* **91**, 3679 (1995).
37. Yagasaki, E., and Masel, R., *Catalysis* **11**, 165 (1994).
38. Zaera, F., and Bernstein, N., *J. Am. Chem. Soc.* **116**, 4881 (1994).
39. Cremer, P., Stanners, C., Niemantsverdriet, J. W., Shen, Y. R., and Somorjai, G., *Surf. Sci.* **328**, 111 (1995).
40. Kovacs, I., and Solymosi, F., *J. Phys. Chem.* **97**, 11056 (1993).
41. Horiuti, J., and Miyahara, K., *NSRDS-NBS* **13** (1968).
42. Horiuti, J., and Polanyi, M., *Trans. Faraday Soc.* **30**, 1164 (1934).
43. Cremer, P. S., and Somorjai, G. A., *J. Chem. Soc. Faraday Trans.* **91**, 3671 (1995).
44. Rekoske, J. E., Cortright, R. D., Goddard, S. A., Sharma, S. B., and Dumesic, J. A., *J. Phys. Chem.* **96**, 1880 (1992).
45. Neurock, M., *in* "Dynamics of Surfaces and Reaction Kinetics in Heterogeneous Catalysis" (G. F. Froment and K. C. Waugh, Eds.), Studies in Surface Science and Catalysis 109. Elsevier Science, Amsterdam/New York, 1997.
46. Neurock, M., and van Santen, R. A., *J. Phys. Chem. B*, in press.
47. Neurock, M., Pallassana, V., and van Santen, R. A., *J. Am. Chem. Soc.*, **122**, 1150 (2000).
48. Saillard, J. S., and Hoffmann, R., *J. Am. Chem. Soc.* **106**, 2006 (1984).
49. Neurock, M., *App. Catal. A: Gen.* **160**, 169 (1997).
50. Neurock, M., and Pallassana, V., *in* "Transition State Modeling for Catalysis" (D. G. Truhlar and K. Morokuma, Eds.), ACS Symposium Series 721, Chapter 18, p. 226. American Chemical Society, Washington, DC, 1999.
51. Whitten, J. L., and Yang, H., *Catal. Today* **50**, 603 (1999).
52. Burghgraef, H., Jansen, A. P. J., and van Santen, R. A., *Chem. Phys.* **177**, 407 (1993).
53. Kratzer, P., Hammer, B., and Nørskov, J. K., *J. Chem. Phys.* **105**, 5595 (1996).
54. Kittel, C., "Introduction to Solid State Physics." John Wiley and Sons, Inc., New York, 1986.
55. Payne, M. C., Teter, M. P., Allan, D. C., Arias, T. A., and Joannopoulos, J. D., *Rev. Mod. Phys.* **64**, 1045 (1992).
56. Kresse, G., and Furthmüller, *Comput. Mater. Sci.* **6**, 15 (1996).
57. Troullier, N., and Martins, J. L., *Phys. Rev. B* **43**, 1993 (1991).
58. Vosko, S. J., Wilk, L., and Nusair, M., *Can. J. Phys.* **58**, 1200 (1980).
59. Hohenberg, P., and Kohn, W., *Phys. Rev. B* **136**, 864 (1964).
60. Kohn, W., and Sham, L. J., *Phys. Rev. A* **140**, 1133 (1965).
61. Perdew, J. P., Chevery, J. A., Vosko, S. H., Jackson, K. A., Pederson, M. R., Singh, D. J., and Fiolhais, C., *Phys. Rev. B* **46**, 6671 (1992).
62. Chadi, D. J., and Cohen, M. L., *Phys. Rev. B* **8**, 5747 (1973).
63. Gillan, M. J., *J. Phys.: Condens. Matter* **1**, 689 (1989).
64. Hammer, B., Hansen, L., and Nørskov, J. K., "DACAPO: A plane-wave, pseudopotential total energy package." Technical University of Denmark, Lyngby, 1995.
65. Hammer, B., Hansen, L. B., and Nørskov, J. K., *Phys. Rev. B* **59**, 7413 (1998).
66. Rodriguez, J. A., *Surf. Sci.* **345**, 347 (1996).
67. Shen, X. Y., Frankel, D. J., Hermanson, J. C., Lapeyre, G. J., and Smith, R. J., *Phys. Rev. B* **32**, 2120 (1985).
68. Heitzinger, J. M., Gebhard, S. C., and Koel, B. E., *J. Phys. Chem.* **97**, 5327 (1993).
69. Hammer, B., and Nørskov, J. K., *in* "Chemisorption and Reactivity on Supported Clusters and Thin Films" (R. M. Lambert, G. Pacchioni, Eds.), p. 285. Kluwer Academic Publishers, Dordrecht, The Netherlands, 1997.
70. Paul, J. F., and Sautet, P., *J. Phys. Chem.* **98**, 10906 (1994).
71. Fahmi, A., and van Santen, R. A., *J. Phys. Chem.* **100**, 5676 (1996).
72. Kesmodel, L. L., and Gates, J. A., *Surf. Sci.* **111**, L747 (1981).
73. Dong, W., Kresse, G., Furthmüller, J., and Hafner, J., *Phys. Rev. B* **54**, 2157 (1996).
74. Paul, J. F., and Sautet, P., *Phys. Rev. B* **53**, 8015 (1996).
75. Paul, J. F., and Sautet, P., *Surf. Sci.* **356**, L403 (1996).
76. "CRC Handbook of Chemistry and Physics," 78th (D. R. Lide, Ed.) CRC Press, Boston, 1998.
77. Dong, W., Kresse, G., and Hafner, J., *J. Mol. Catal. A: Chem.* **119**, 69 (1997).
78. Conrad, H., Ertl, G., and Latta, E. E., *Surf. Sci.* **41**, 435 (1974).
79. Hammer, B., and Nørskov, J. K., *Nature* **376**, 238 (1995).
80. Hammer, B., and Nørskov, J. K., *Surf. Sci.* **343**, 211 (1995).
81. Gates, B. C., "Catalytic Chemistry." John Wiley and Sons, Inc., New York, 1992.
82. Hammond, G. S., *J. Am. Chem. Soc.* **77**, 334 (1955).
83. Boudart, M., and Djega-Mariadassou, G., "Kinetics of Heterogeneous Catalytic Reactions." Princeton University Press, Princeton, NJ, 1984.
84. Hammer, B., Nielsen, O. H., and Nørskov, J. K., *Catal. Lett.* **46**, 31 (1997).
85. Newns, D. M., *Phys. Rev. B* **178**, 1123 (1969).
86. Brivio, G. P., and Trioni, M. I., *Rev. Mod. Phys.* **71**, 231 (1999).
87. van Santen, R. A., and Neurock, M., *Catal. Rev.* **37**, 557 (1995).
88. Hammett, L. P., *J. Am. Chem. Soc.* **59**, 96 (1937).
89. Lowry, T. H., and Richardson, K. S., "Mechanism and Theory in Organic Chemistry." Harper & Row, New York, 1987.
90. Hoffmann, R., "Solids and Surfaces, A chemist's view of bonding in extended surfaces." VCH, New York, 1988.
91. Hoffmann, R., *Angew. Chem. Tnt. Ed. Engl.* **21**, 711 (1982).